Ce-promoted Fe–Cu–ZSM-5 catalyst: SCR-NO activity and hydrothermal stability

Houda Jouini, Imène Mejri, Baker Rhimi, Mourad Mhamdi, Teresa Blasco, Gérard Delahay

Ce-promoted Fe-Cu-ZSM-5 catalyst: SCR-NO activity and hydrothermal stability

Houda Jouini[1,2] · Imène Mejri[1,2] · Baker Rhimi[3] · Mourad Mhamdi[1,2] Teresa Blasco[4] · Gérard Delahay[5]

[1] LR01ES08 Laboratoire de Chimie des Matériaux et Catalyse, Faculté des Sciences de Tunis, Université de Tunis El Manar, 2092 Tunis, Tunisie

[2] Institut Supérieur Des Technologies Médicales de Tunis, Université de Tunis El Manar, 1006 Tunis, Tunisie

[3] School of Environmental Science and Engineering, Shaanxi University of Science and Technology, Xi'an, Shaanxi 710021, People's Republic of China

[4] Instituto de Tecnología Química, Universitat Politècnica de València - Consejo Superior de Investigaciones Científicas (UPV-CSIC), Avda. de los Naranjos s/n, 46022 Valencia, Spain

[5] ICGM, ENSCM (MACS), CNRS, Univ Montpellier, Montpellier, France

Houda Jouini,+216 99 92 56 55, houda.jouini@fst.utm.tn

Abstract Fe-Cu-ZSM-5 and Ce-Fe-Cu-ZSM-5 solids prepared using solid-state ion exchange method (SSIE) were tested in the NH_3-SCR of NO reaction and were characterized using N_2 physisorption at 77 K, MAS ^{27}Al magnetic resonance, X-ray diffraction, scanning electron microscopy, EPR spectroscopy and transmission electron microscopy coupled to energy dispersive X-ray spectroscopy in order to follow the effect of Ce addition on the textural and structural properties of Fe-Cu-MFI system as well as the detection of the changes in local environment and state of iron and copper species, and the degradation of the zeolite texture and structure after a severe aging treatment at 850 °C for 5h. Fresh Ce-promoted sample showed better NO conversion up to 450 °C than unpromoted Fe-Cu-ZSM-5 catalyst. An activity loss was observed on aged catalysts, but remaining less pronounced for the catalyst

containing Ce. The changes in catalyst structure and texture did not occur during aging while a probable migration of metal active species and change in their coordination has occurred.

Keywords Cerium · SSIE · SCR · NO · ZSM-5

Introduction

Motorized transport is one of the main sources of air pollution. Automotive pollution problems in terms of air quality have prompted researchers worldwide to devote innovative solutions to air pollutants abatement. The progressive implementation of these solutions has made major advances in the cause. However, the number of motor vehicles continues to grow, especially in countries of rapid industrialization. Facing this growth, the United States, Europe and Japan are adopting increasingly stringent pollution standards [1-3], while at the same time the standards introduced in these countries are being gradually taken over by other ones. In the European Union, road vehicles are the most important source for the emissions of air pollutants. The Euro standards were designed to reduce these emissions considerably and among all pollutants, more attention should be paid to nitrogen oxides (NOx), as they are responsible for a wide variety of serious health and environmental problems. As legislation is becoming stricter, a better understanding of the catalytic materials and further development of adequate DeNOx technologies are required.

Metal-exchanged zeolites, in particular with iron and copper, are well known catalysts for the SCR-NOx in the presence of ammonia used as a reducing agent, a widely used pollution control technology for removing exhaust nitrogen oxides generated from power plants, ships and vehicles to the emission levels required by legislation [4]. Fe-Cu-ZSM-5 catalytic system has proven its efficiency in NOx abatement in a wide temperature window (180-550°C) [5-9]. To be an interesting candidate for automotive Diesel applications, such catalyst must support the severe conditions of vehicle engine and show a high hydrothermal stability up to 800 °C

[10-14]. Recently, Ce-based catalysts [15-18] have also received considerable attention for NO removal through the NH_3-SCR process thanks to its single properties to combine elevated oxygen transport capacity and to shift easily between Ce^{4+}/Ce^{3+} reduced and oxidized states [19-21]. Since cerium species are known to favour the oxidation of NO to NO_2, considered as the key step of the standard NH_3-SCR reaction in the presence of O_2, Ce-promoted zeolites seems to be promising catalysts for NO abatement through the SCR process [11].

Both copper and iron zeolites catalysts are widely used in automotive industry [22,23], and in particular, SSZ-13 and SAPO-34 as host structures [24-26]. Nevertheless, improvements are still necessary and in particular, the DeNOx performances at low temperatures (<250 ° C) and the maintenance of the NOx reduction activity with the time on stream (> 160,000 km).

The aim of this study is to upgrade the catalytic activity of Fe-Cu-ZSM-5 SCR-catalyst by adding cerium as a promoter and to elucidate the outcome of high temperature hydrothermal aging on the structure, texture and catalytic activity of both promoted and unpromoted catalysts.

Experimental

Catalysts Preparation

The desired catalysts with the following theoretical composition Ce (0.5wt.%)-Fe (2wt.%)-Cu (1.5wt.%)-ZSM-5 and Fe (2wt.%)-Cu (1.5wt.%)-ZSM-5, were prepared by consecutive-step solid-state ion exchange (SSIE) as follow:

Fe-Cu-ZSM-5 catalyst was prepared as follow: 1 g of zeolite was mixed and finely ground with the desired amount of $CuCl_2*2H_2O$ in an agate mortar for 5 min under ambient conditions. The resulting mixture was then treated under a stream of helium (99.99%, Air Liquide, 30 cm^3 min-1) for 12 h at 380 °C (2 °C min-1). The obtained powder was mixed and finely ground with the desired amount of $FeCl_2*6H_2O$, then heated for 12 h at 290 °C in a stream of helium and under the same conditions described previously.

Ce-Fe-Cu-ZSM-5 catalyst was prepared by adding a third step, which consists in mixing Fe-Cu-ZSM-5 solid with 0.5 wt.% of cerium chloride ($CeCl_3*7H_2O$, Sigma-Aldrich) by mechanical grinding in an agate mortar. The mixture was finally treated at 500 °C for 12h in a stream of helium with a flow rate of 30 cm^3/min and a heating rate of 1°C/min for 12 hours.

The prepared catalysts were labelled as Fe-Cu-Z and Ce-Fe-Cu-Z where Z is the ZSM-5 support.

Catalysts aging

The aging conditions were chosen according to previous works [27-29]. An amount of 200 mg of catalyst is deposited on a porous frit of a U-tube quartz reactor in which a gas flow (20% O_2 / He) of 50 cm^3/min circulates. Then, the reactor is heated to 850 °C with a ramp of 6 °C/min. The injection of H_2O (liq.) (0.0041 cm^3 / min), by a syringe pump is started and maintained at this temperature for 5 h. Finally, the oven is cooled to room temperature and the water injection is stopped during the cooling procedure once the temperature reaches 450 °C. The aged catalysts were labelled Fe-Cu-Zag and Ce-Fe-Cu-Zag.

Physical and chemical characterization

The chemical analysis of the studied materials was carried out by ICP-AES in a Varian 715-ES. The wavelengths used for Cu and Fe analysis were 327.395 and 234.350 nm, respectively. The samples crystallinity was checked using a PANanlytical Cubix'Pro diffractometer equipped with an X'Celerator detector and automatic divergence and reception slits using Cu-Kα radiation (0.154056 nm). The equipment is working under a voltage of 45 kV and a current of 40 mA. The diffractograms were recorded in the region of 5-40 ° and were exploited with the software PANalytical X'Pert HighScore Plus. Textural properties of the samples were determined by N_2-physisorpton at 77 K using a Micromeritics ASAP 2000 instrument. The samples were previously degassed for 5 h at 250 °C. The morphology of samples was observed by Field Emission Scanning Electron Microscopy a ZEISS AURIGA

55 Compact instrument in combination with an EDX detector. The sample powder was deposited in double-sided tape and analysed without metal covering. The solid-state NMR spectra were recorded at room temperature under magic angle spinning (MAS) in a Bruker WB spectrometer. The ^{27}Al MAS NMR spectra were recorded using a BL-4probe with 4mm diameter zirconia rotors spinning at 104.21 MHz. The ^{27}Al spectra were referred to 0.1M dissolution of $Al(NO_3)_3$. EPR spectra were recorded at 105 K on a Bruker EMX-12 spectrometer operating in the X band with a frequency and an amplitude modulation of 100 kHz and 1.0 Gauss respectively. STEM observations were performed using a JEOL-JEM 2100F instrument equipped with an X-MAX microanalysis detector and operating under an accelerating voltage of 200 kV and resolution energy of 20 eV.

Catalytic testing

The NH_3-SCR of NO catalytic test was performed in temperature programmed surface reaction (TPSR) using a flow reactor operating at atmospheric pressure with a space velocity of 333.333 h^{-1} and a total flow rate of 6 L h^{-1}. 18 mg of each sample were activated in-situ at 250 °C under oxygen and helium mixture (3.5% H_2O, 8% O_2 and 88.3% He) and then cooled to 50 °C. The samples were tested from 200 °C to 550 °C under the same H_2O/O_2/He atmosphere and using the following gas composition: 1000 ppm of NO and 1000 ppm of NH_3. The reaction gas mixture was admitted to the reactor with the aid of mass flow controllers. The effluent composition was continuously monitored and by sampling on line to a quadruple mass spectrometer (Omnistar Pfeiffer Vacuum) equipped with Channeltron and Faraday detectors. Catalytic results were expressed as follows:

$X_{NO} = \frac{[NO_0]-[NO_T]}{[NO_0]} \times 100$, where $[NO_0]$ and $[NO_T]$ are the concentrations of NO at the inlet gas reactor and at the temperature T, respectively.

Results and discussion

Characterisation results

The chemical analysis of prepared solids was carried out by ICP-AES technique, Table 1 gathers the contents of Fe, Cu and Ce expressed in wt.% as well as the X/Al (X=Si, Cu, Fe and Ce) molar ratios. Examination of ICP results shows that metals are well retained by the zeolite during the preparation process where the experimental amounts approximate the theoretical values set for the catalysts preparation. This result is expected since the SSIE is the most convenient method for controlling the metal amount in the prepared solids, which is in perfect agreement with our previous works [12-14]. The ratio of the parent zeolite stated by Zeolyst (CBV024E, Si/Al=15) was decreased in the case of prepared catalysts and that can be attributed to the reproducibility of routine sequential syntheses which may vary from batch to batch [30].

Table 1 ICP-AES chemical analysis results

N_2 physisorption at 77 K experiments showed that all the prepared samples are microporous with BET surface areas (Table 2) between 327 and 317 m^2/g depending mainly on the composition and the thermal treatment of each sample. For the Fe-Cu-Zag sample, a slight decrease of the BET surface (11%) and the micropore volume (58%) compared to the fresh sample were observed evidencing a probable occlusions of the zeolite pores by an agglomerated phase. After hydrothermal treatment, the Ce-promoted sample has retained its pore volume and even slightly improved its S_{BET}.

Table 2 N_2 physisorption at 77 K results.

The porosity of zeolite nanoparticles before and after aging treatment was investigated by N_2 sorption analysis (Fig.1). The shapes of nitrogen adsorption-desorption isotherms showed the typical Type H3 loop in the case of fresh samples while aged samples showed the Type H4 loop according to the classification of IUPAC [iupac]indicating the presence of mesoporosity formed by the packing of zeolite nanocrystals [16]. The hysteresis loops of the fresh samples

are larger than those of aged samples, suggesting implying that hydrothermal treatment affects the pore shapes of the ZSM-5. The BET suraface areas of the studied samples are presented in Table 1 and a decrease of about 11% was found for the Fe-Cu-Zag catalyst. After hydrothermal treatment, Ce-based catalyst has retained and even improved its S_{BET} of 3% suggesting a partial modification of the external surface. The textural properties were overall maintained after hydrothermal treatment at 850 °C hence excluding any hydrothermal instability.

Fig. 1 N_2 Adsorption-desorption isotherms of fresh and aged catalysts.

XRD characterisation shows the typical diffraction patterns of the ZSM-5 (MFI) structure in all the prepared samples (Fig. 2). The introduction of metals (Fe, Cu and Ce) did not modify the zeolite crystal structure and added no new diffraction peaks, which is expected given the low metal content of the samples (0.5-1.5 wt.%). XRD diffractograms of the aged catalysts showed a weak decease of the peaks intensity with the absence of any extra-framework metal phases or any sign of a probable amorphization. This feature can be explained by the removal of a small amount of Al atoms from the framework without the destruction of the structure due to the hydrothermal treatment.

Fig. 2 XRD diffractograms of parent zeolite and prepared catalysts.

This finding was confirmed by FE-SEM observations (Fig. 3), showing for both fresh and aged samples well-crystallised zeolite particles of rectangular prism shapes with an average length of 100 nm and an average width and thickness of 57 nm. The metal particles were not observed in this magnification due to their small amount. From this analysis we demonstrate that the aged catalysts have the same morphology of the fresh zeolite crystals, without any detected agglomeration.

Fig. 3 3 FE-SEM micrographs of (a) Fe-Cu-Z, (b) Fe-Cu-Zag, (c) Ce-Fe-Cu-Z and (d) Ce-Fe-Cu-Zag catalysts.

Solid-state MAS ^{27}Al-NMR spectroscopy was implemented to probe the structural ordering and the coordination of aluminium after steam treatment of SSIE and aging. The recorded spectra are presented in Fig.4.

All spectra of studied catalysts exhibit a dominant resonance at around 54 ppm assigned to framework aluminium in lattice positions (tetrahedrally coordinated Al). The intensity of this peak is reduced after aging, this may suggest that the steam treatment distorted the coordination of framework Al species, some of those species may become NMR-silent due to their lower symmetry [31]. A small contribution is recorded at 0 ppm showing the presence of extra-framework aluminium species (EFAL) in octahedral symmetry. The intensity of EFAL peak did not increase for the spectra of aged samples indicating that no probable dealumination has occurred which is in line with the results of XRD and FE-SEM techniques. In fact, the intensity of EFAL peak has rather decreased, it may be explained by a healing process based on a migration of EFAL atoms to framework vacancies and their transformation to AlO_4 species [27,32]. Perhaps steam treatment at 850 °C under inert gas for 5 hours allows this reintegration. On the other hand, Fig. 4 shows that the hydrothermal treatment at 850 °C had little affected the zeolite structure.

Fig. 4 ^{27}Al NMR spectra of fresh and aged (a) Fe-Cu-Z and (b) Ce-Fe-Cu-Z.

In order to analyse the nature and distribution of metallic species in the studied samples, EPR spectroscopy experiments were conducted at 105 K (Fig. 5).

Fig. 5 EPR spectra of fresh and aged catalysts.

Fresh and aged samples exhibit an axial EPR spectrum of isolated Cu^{2+} species (I=3/2) with resolved hyperfine structure (HFS) with $g_{\parallel}$= 2.38 and $g_{\perp}$ = 2.09 as shown in Fig.5b. CuO species with strong antiferromagnetic coupling are EPR silent [33]. The EPR signal of Fe-Cu-Z was modified after hydrothermal treatment indicating a change in the local environment of Cu^{2+} cations whereas no appreciable changes were detected for Ce-Fe-Cu-Z suggesting that the presence of Ce stabilizes the Cu^{2+} sites. A strong line was also observed for all analysed samples at g=4.3 (Fig. 5a) and was assigned to isolated Fe^{3+} ions in tetrahedral coordination [34]. It was however difficult to detect the Fe^{3+} of oxide clusters FeOx as the corresponding signal (g=2) could be hidden by the broad and intense signal of isolated Cu^{2+} ($g_{\perp}$=2.09) [35]. Fig 5.a also shows that Fe-Cu-Z catalyst exhibits two additional signals at g=5.6 and g=6 both assigned to highly coordinated Fe^{3+} ions [36].

After the addition of Ce, EPR spectra reveal a decrease in the intensity of tetrahedral Fe^{3+} signal and the disappearance of the two signals related to highly coordinated ferric ions. Thus, we can conclude that the presence of Ce stabilizes iron ions in the tetrahedral symmetry. Unlike the Fe-Cu-Z sample, the EPR signal of Ce-Fe-Cu-Z at g=4.3 remain practically unchanged after aging confirming again the stabilizing effect of cerium for metal sites during steam treatment.

Several STEM observations have been conducted on the fresh samples (Fig. 6). The distribution of Fe, Cu and Ce species was confirmed by EDX elemental analysis (Table 3). The STEM image of Fe-Cu-Z (Fig. 6a) shows a limited number of Fe-Cu nanocomposites (spectrum 22) with an average size of 7 nm. Iron particles are also present with a larger size (5-20 nm). In the case of Ce-Fe-Cu-Z (Fig. 6b), a limited number of large copper particles (spectrum 38) is observed with a maximum size up to 60 nm. They coexist with smaller iron nanoparticles (6-12 nm).

Table 3 EDX elemental analysis results

Cerium particles could not be seen directly in the STEM micrographs, but the presence of Ce was verified by means of EDX mapping indicating for the sample Ce-Fe-Cu-Z that Ce species were nanosized (<100 nm) and highly dispersed on the catalyst surface. EDX mapping images also showed that the addition of cerium ameliorates the dispersion of Fe species and promotes the aggregation of copper species in the Cu-Fe-Z solid ; the size of iron particles is reduced with a rather uniform distribution.

Fig. 6 STEM and EDX mapping micrographs of (a) Fe-Cu-Z and (b) Ce-Fe-Cu-Z catalysts.

Fig. 7 EDX-STEM mapping images of (a) Fe-Cu-Z and (b) Ce-Fe-Cu-Z catalysts.

Catalytic results

Fresh and aged catalysts were tested in the NH_3-SCR of NO reaction, the obtained NO conversion profiles are shown in Fig. 7.

Fig. 8 NO conversion over fresh and aged catalysts.

Catalytic tests show that NO conversion at low temperature range is higher (50% at 240 °C and 100% at 315 °C) for Ce-Fe-Cu-Z catalyst than for Fe-Cu-Z catalyst (50% at 272 °C and 100% at 401 °C). This result supports the fact that Ce favours the oxidation of NO into NO_2 considered as the first step in the standard NH_3-SCR reaction. The main reason is that cerium exhibits a unique combination of elevated oxygen transport capacity and an ability to shift easily between its two oxidation states +III and +IV [19, 37]. These characteristics favour the oxygen adsorption on the catalyst surface and lead to the formation of chemisorbed oxygen. Such species are known to play an important role in NH_3-SCR redox mechanism as it was reported in the literature [10]. The high concentration of highly dispersed nano-crystalline cerium should be also the reason for the excellent performance of the Ce-Fe-Cu-Z catalyst [20].

Above 480 °C the NO conversion of Ce-Fe-Cu-Z catalyst notably decreases in comparison with the unpromoted sample, such behaviour is explained by to the over-oxidation of NH_3 to NO, which is in perfect agreement with previous studies reporting that the addition of Ce increases the oxidation of NH_3 [19]. Other studies have proven that such reaction is promoted by the presence of large metal oxide particles, mainly CuO_x [12]. In accordance with this and as observed in the STEM micrograph of Ce-Fe-Cu-Z, the degree of aggregation of Cu has increased, which explains the highest activity of the latter catalyst in the ammonia oxidation reaction. It is commonly accepted that isolated Fe^{2+} and Fe^{3+} ions are the main iron active sites involve in the NH_3-SCR of NO mechanism [38], small iron clusters were also found to be active sites [39]. Boroń reported that tetrahedrally-coordinated Fe^{3+} ions (a species detected by EPR in all the studied samples), are responsible for the high activity of the Fe-based zeolite catalysts in the high temperature region [40]. We have shown that the addition of cerium promoted the dispersion of iron leading to smaller iron nanosized particles and stabilized iron ions in the tetrahedral symmetry leading the highest activity of Ce-promoted catalyst in the studied reaction. On the other hand, it has been suggested in the literature that the Cu^{2+} ions and copper oxo cations play a crucial role in the NH_3-SCR reaction below 300 °C, while above 350 °C, all copper ions become active [41,42]. Dou et al found that the addition of cerium improved the redox properties of the Cu/ZSM-5 catalysts due to the higher valence of copper and mobility of lattice oxygen leading to an enhanced low-temperature SCR activity which is in perfect agreement with our catalytic results [43].

STEM observations showed that in the presence of Ce, the degree of aggregation of Cu increased and large copper aggregated with a size up to 60 nm are formed. This finding may explain the decrease of NO conversion for Ce-Fe-Cu-Z at above 480 °C, since the transition metal oxides and mainly Cu particles are known to catalyze the selective catalytic oxidation of NH_3 (NH_3-SCO) [44,45].

After the hydrothermal treatment, an important deactivation is observed over the total temperature window for the steamed samples and is more significant for the unpromoted catalyst. The NO conversion of both aged catalysts begins at 200 °C and was nearly the same (30 %), then surprisingly decreases to reach a minimum of 0 and 16 % of NO conversion for Ce-Fe-Cu-Zag and Fe-Cu-Zag respectively at around 300 °C. Above this temperature, a large improvement of the conversion is observed and the maximum of NO conversion of 63 and 72% is obtained at 550 °C for Ce-Fe-Cu-Zag and Fe-Cu-Zag, respectively.

Fig. 9 N_2 selectivity over fresh and aged catalysts.

All supports were selective toward N_2 with a selectivity exceeding 90% over the entire temperature range with a maximum of 98 % (Fig. 9). The yield of N_2 has deteriorated to reach a minimum of 93 % in the presence of both aged catalysts at around 360 °C and 527 °C for Fe-Cu-Zag and C-Fe-Cu-Zag, respectively.

Regarding the loss of activity after aging, two possibilities that are usually encountered in the literature under similar aging conditions : (1) dealumination and loss of the zeolite structure and therefore loss of the textural preoperties, or (2) no dealumination but agglomeration/ and or migration of the metal cations and alteration of catalytic sites. Brandeberger et al studied the deactivation of Fe/ZSM-5 system for the NH_3-SCR of NO [46]. Their results showed that the main cause of hydrothermal aging is Fe migration leading to the formation of FeOx clusters. It was found that this Fe migration was not strongly related to the process of dealumination and the SCR activity depends more on the stability of the active iron species in ion exchange sites than the stability of the framework. Brandenberger and his team showed also is this study that aging at 800 °C for 8 h resulted in only a small decrease in the BET surface area, which is in agreement with our N_2 physisorption results. Porous structure of the zeolite was found intact after hydrothermal aging due to the stability of the Si–O–Si bond, which does not degrade to a significant extent.

As the structural and textural stability were maintained after the hydrothermal treatment in our case as shown by N_2 physisorption, XRD, FE-SEM and ^{27}Al NMR techniques, the deactivation of the studied catalysts is then a matter of the modification of the metal sites catalysing the SCR reaction.

Other research groups studiying the deactivation of Cu/ZSM-5 system showed that the catalytic activity of Cu-ZSM-5 was lost because of Cu ion migration and change in Cu^{2+} coordination while the zeolite framework remained less affected [47,48]. The reactivity of these altered Cu^{2+} sites and their ability to adsorb different molecules was substantially affected. Since Cu^{2+} ions are known as the main active species for low-temperature SCR reaction, the latter findings may explain the severe activity deterioration of Fe-Cu-Zag catalyst. Ce-Fe-Cu-Zag catalyst showed less deactivation during the SCR reaction than Fe-Cu-Zag, thanks to the presence of Ce which stabilized the Cu^{2+} sites and Fe^{3+} ions in the tetrahedral symmetry as shown in EPR study.

Conclusion

Ce-Fe-Cu-ZSM-5 and Fe-Cu-ZSM-5 catalysts were prepared by SSIE method and tested in the SCR-NO reaction in the presence of NH_3. The combination of copper, iron and cerium significantly enhanced the low temperature SCR activity. Cerium acts as the oxygen storage promoter and enhances the oxidation of NO to NO_2 known as the key step for the NH_3-SCR mechanism for NO abatement in the presence of O_2 but also favours the oxidation of ammonia hence the decrease in the activity of the Ce-promoted catalyst at high temperature range. A similar-trend deactivation of both the Fe-Cu-ZSM-5 and Ce-Fe-Cu-ZSM-5 has occurred after the aging process at 850 °C for 5h with some differences in the extent of the deactivation between those samples. The deactivation is more severe in the case of the unpromoted catalyst. Aged Ce-Fe-Cu-ZSM-5 showed a better catalytic activity owing to the

presence of Ce species which helped to stabilize the catalytic sites during the hydrothermal treatment. Neither significant structural and textural changes nor severe dealumination of the zeolite were detected for our catalysts, indicating that deactivation was caused only by changes in the distribution and coordination of iron and/or copper active sites.

Acknowledgments

Financial support by the MINECO of Spain through the Severo Ochoa (SEV-2016-0683) and RTI2018-101784-B-I00 projects is gratefully acknowledged.

References

1. Winkler SL, Anderson JE, Garza L, Ruona1 WC, Vogt R, Wallington TJ (2018) Clim Atmos Sci 1: 26-30

2. Hooftman N, Messagie M, Van Mierlo J, Coosemans T (2018) Renewable Sustainable Energy Rev 86: 1-21

3. Shigeta N, Hosseini SE (2021) Energies 14: 78-109

4. Li J, Chang H, Ma L, Hao J, Yang RT (2011) Catal Today 175: 147-156

5. Sultana A, Sasaki M, Suzuki K, Hamada H (2013) Catal Comm 41: 21-25

6. Nakhostin Panahi P, Salari D, Niaei A, Mousavi SM (2013) J Ind Eng Chem 19: 1793-1799

7. Yue Y, Liu B, Lv N, Wang T, Bi X, Zhu H, Yuan P, Bai Z, Cui Q, Bao X (2019) Chem Cat Chem 11: 4744-4754

8. Liu Q, Bian C, Ming S, Guo L, Zhang S, Pang L, Liu P, Chen Z, Li T (2020) Appl Catal A Gen 607: 117865

9. Doan T, Dam P, Nguyen K, Vuong TH, Le MT, Pham TH (2020) Catalysts 10: 321-341.

10. Zhang T, Liu J, Wang D, Zhao Z, Wei Y, Cheng K, Jiang G, Duan A (2014) Appl Catal B Environ 148-149: 520-531

11. Qi G, Yang RT (2004) J Phys Chem B 108: 15738-15747

12. Jouini H, Martinez-Ortigosa J, Mejri I, Mhamdi M, Blasco T, Delahay G (2019) Res Chem Intermed 45: 1057-1072

13. Jouini H, Mejri I, Martinez-Ortigosa J, Vidal-Moya A, Mhamdi M, Blasco T, Delahay G (2018) Microporous Mesoporous Mater 260:217-226

14. Jouini H, Mejri I, Martinez-Ortigosa J, Cerrillo JL, A, Mhamdi M, Palomares AE, Delahay G, Blasco T (2018) Solid State Sci 84: 75-85

15. Xu J, Yu H, Zhang C, Guo F, Xie J (2019) New J Chem 43: 3996-4007

16. Abid R, Delahay G, Tounsi H (2019) J Rare Earths 38:250-256

17. Yan L, Ji Y, Wang P, Feng C, Han L, Li H, Yan T, Shi L, Zhang D (2020) Environ Sci Technol 54: 9132-9141

18. Zhou J, Guo R, Zhang X, Liu Y, Duan C, Wu G, Pan W (2021) Energy Fuels 35 (2021) 2981-2998

19. Zhou G, Zhong B, Wang W, Guan X, Huang B, Ye D (2011) Catal Today 175: 157-163

20. Gao X, Jiang Y, Fu Y, Zhong Y, Luo Z, Cen K (2010) Catal Commun 11: 465-469

21. Wang P, Yan L, Gu Y, Kuboon S, Li H, Yan T, Shi L, Zhang D (2020) Environ Sci Technol 54: 6396–6405

22. Johnson TV, Joshi A (2018) Catalysis Book Series: NOx Trap Catalysts and Technologies Fundamentals and Industrial Applications 1-35

23. Maizak D, Wilberforce T, Olabib AG (2020) Environ Adv 2: 100021

24. Gao F, Kwak JH, Szanyi J, Peden, CHF (2013) Top Catal 56:1441-1459

25. Beale AM, Gao F, Lezcano-Gonzalez I, Peden CHF, Szanyi J (2015) Chem Soc Rev 44:7371-7405

26. Urrutxua M, Pereda-Ayo B, De-La-Torre U, González-Velasco JR (2019) ACS Omega 4 :14699-14713

27. Petitto C, Delahay G (2015) Chem Eng J 264: 404-410

28. Martín N, Vennestrøm PNR, Thogersen JR, Moliner M, Corma A (2017) Chem Eur J 23: 13404-13414

29. Shan Y, Du J, Yu Y, Shan W, Shi X, He H (2020) Appl Catal B Environ 266: 118655

30. Shelyapina MG, Krylova EA, Zhukov YM, Zvereva IA, Rodriguez-Iznaga I, Petranovskii V, Fuentes-Moyado S (2019) Molecules 2019, 24, 4216

31. Jia J, Sun Q, Wen B, Chen LX, Sachtler WMH (2002) Catal Lett 82: 7-11

32. Jacobsen CJH, Madsen C, Janssens TVW, Jakobsen HJ, Skibsted J (2000) Microporous Mesoporous Mater 39: 393-401

33. Kouwenhoven HW (1973) Adv Chem 121: 529-539

34. Schwidder M, Kumar MS, Klementiev K, Pohl MM, Brückner A, Grünert W (2005) J Catal 231: 314-330

35. Kumar MS, Schwidder M, Grünert W, Bentrup U, Brückner A (2006) J Catal 239: 173-186

36. Beznis NV, Weckhuysen BM, Bitter JH (2010) Catal Lett 138: 14-22

37. Trovarelli A, Boaro M, Rocchini E, Leitenburg C, Dolcetti G (2001) J Alloy Comp 323-324: 584-591

38. Brandenberger S, Kröcher O, Tissler A, Althoff R (2008) Catal Rev Sci Eng 50: 4925-31

39. Brandenberger S, Kröcher O, Tissler A, Althoff R (2010) Appl Catal B Environ 95: 348-357

40. Boroń P, Chmielarz L, Dzwigaj S (2015) Appl Catal B Environ 168-169: 377-384

41. Matsumoto S, Yokota K, Doi H, Kimura M, Sekizawa K, Kasahara S (1994) Catal Today 22:127-146

42. Kieger S, Delahay G, Coq B, Neveu B (1999) J Catal. 183: 267-280

43. Dou B, Lv G, Wang C, Hao Q, Hui K (2015) Chem Eng J 270 : 549-556

44. Lietti L, Ramirez G, Busca G, Bregani F, Forzatti P (2000) Catal Today 61:187-195

45. Chmielarz L, Kuśtrowski P, Rafalska-Łasocha A, Dziembaj R (2005) Appl Catal B Environ 58: 235-244

46. Brandenberger S, Kröcher O, Casapu M, Tissler A, Althoff R (2011) Environ 101: 649-659

47. Gómez SA, Campero A, MartÍnez-Hernández A, Fuentes GA App Catal A Gen (2000) 197: 157-164

48. Kucherov AV, Hubbard CP, Shelef M (1995) J Catal 157 : 603-610

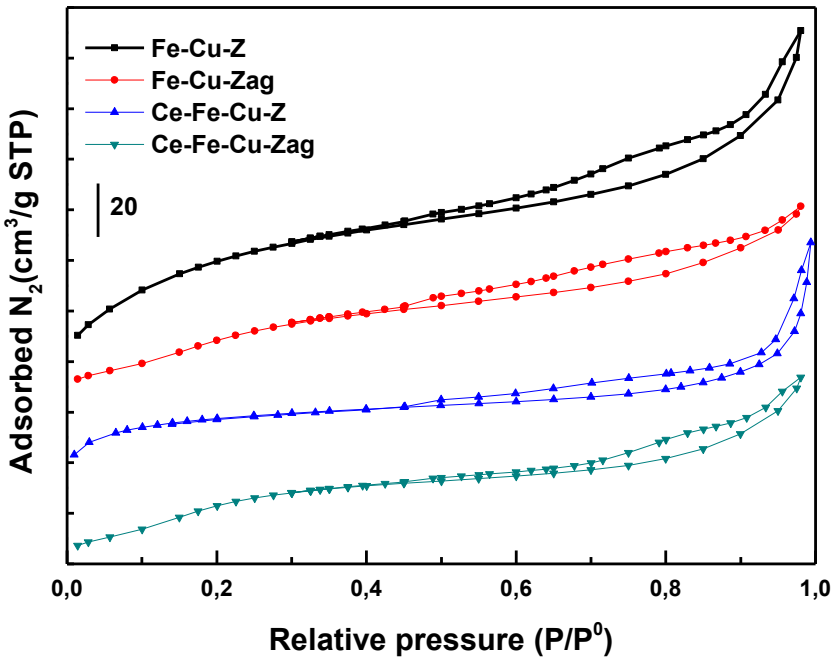

Fig. 1 N_2 Adsorption-desorption isotherms of fresh and aged catalysts.

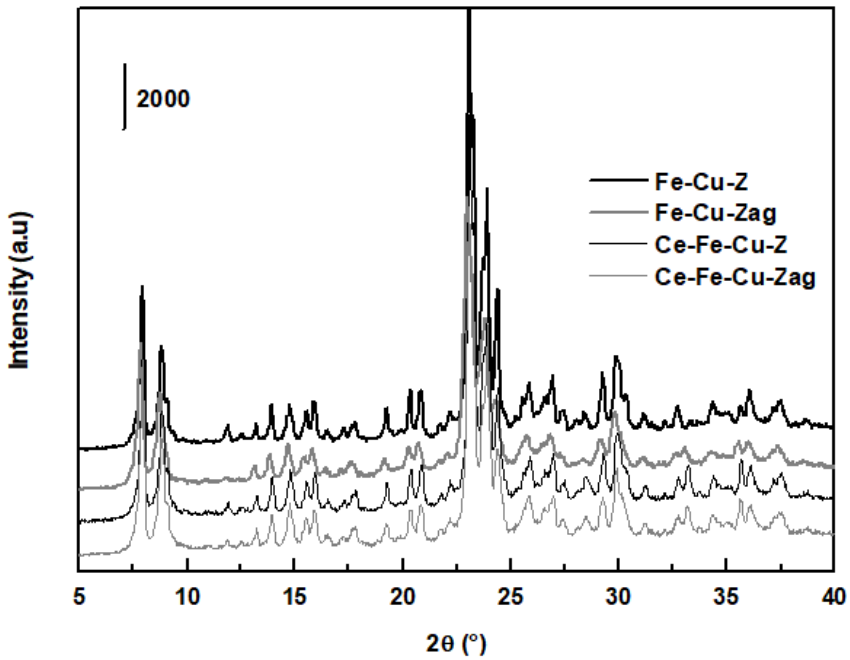

Fig. 2 XRD diffractograms of parent zeolite and prepared catalysts.

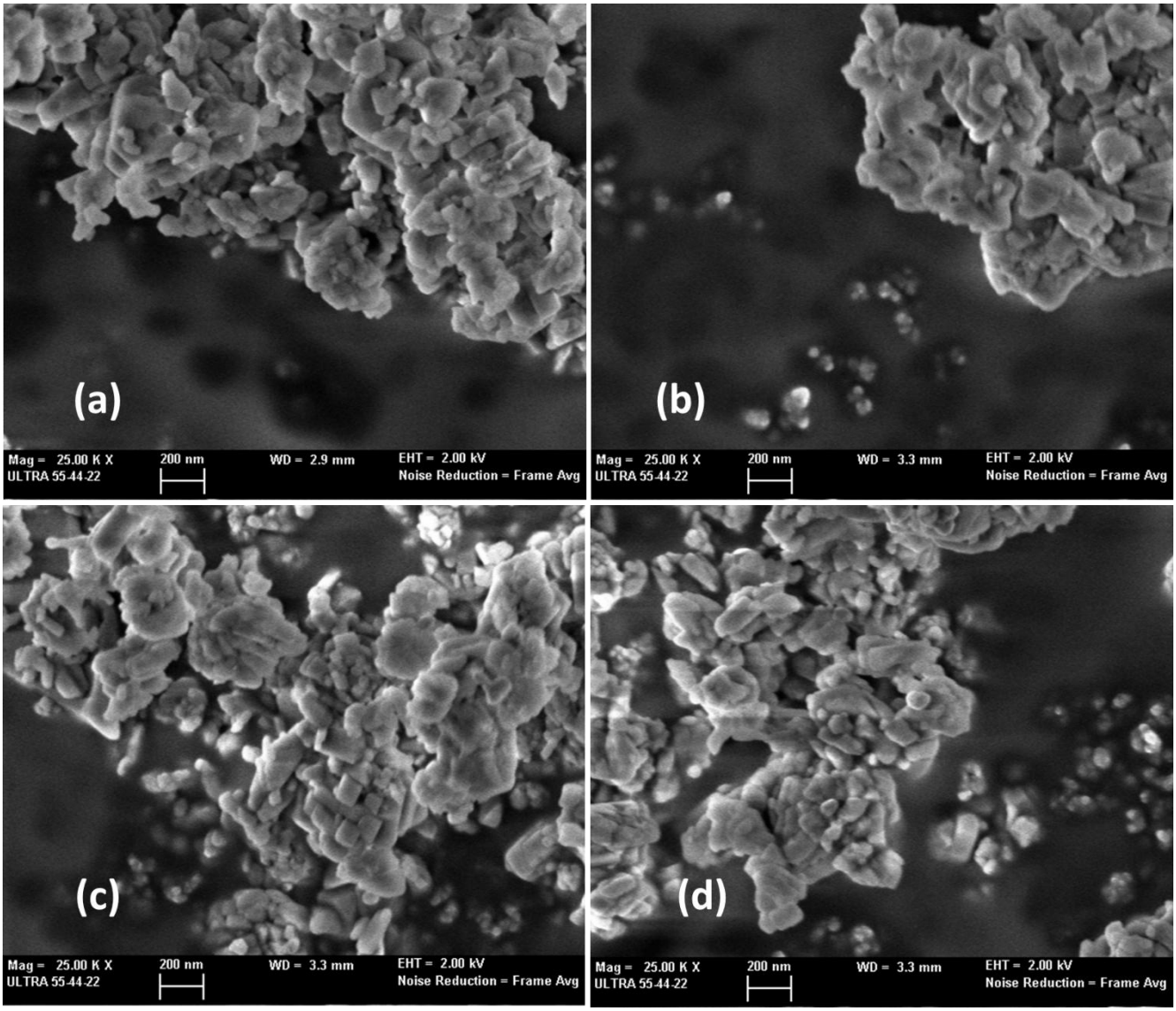

Fig. 3 FE-SEM micrographs of (a) Fe-Cu-Z, (b) Fe-Cu-Zag, (c) Ce-Fe-Cu-Z and (d) Ce-Fe-Cu-Zag catalysts.

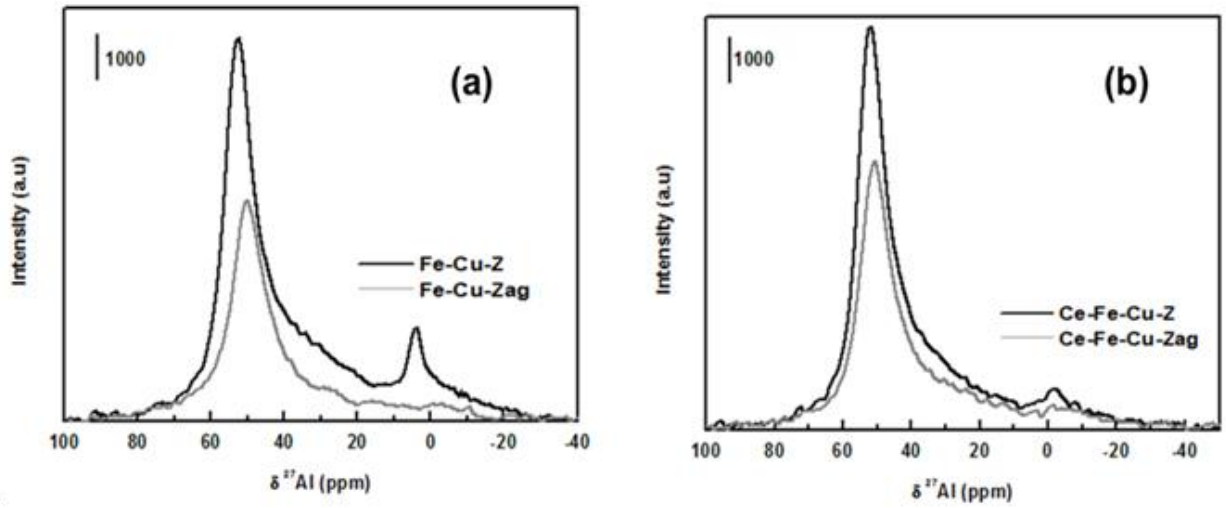

Fig. 4 ^{27}Al NMR spectra of fresh and aged (a) Fe-Cu-Z and (b) Ce-Fe-Cu-Z.

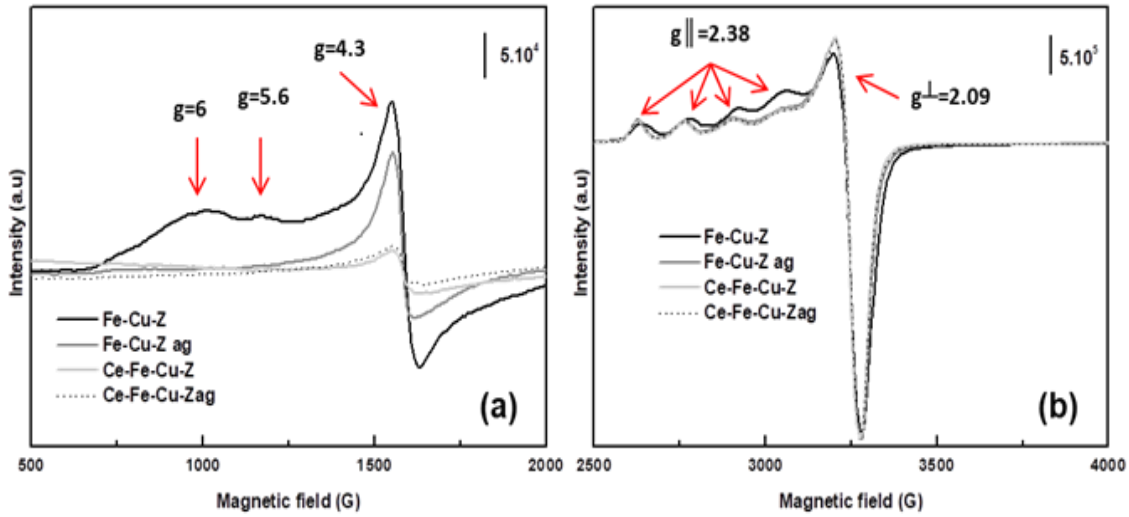

Fig. 5 EPR spectra of fresh and aged catalysts.

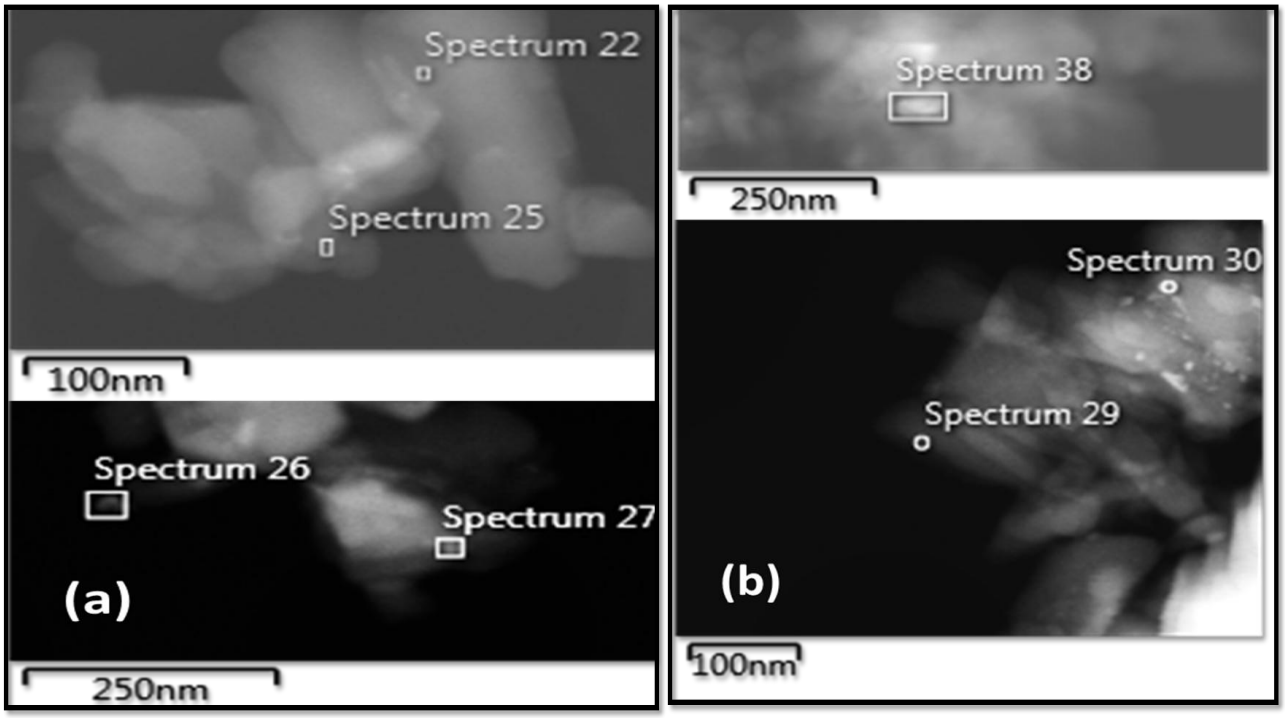

Fig. 6 STEM micrographs of (a) Fe-Cu-Z and (b) Ce-Fe-Cu-Z catalysts.

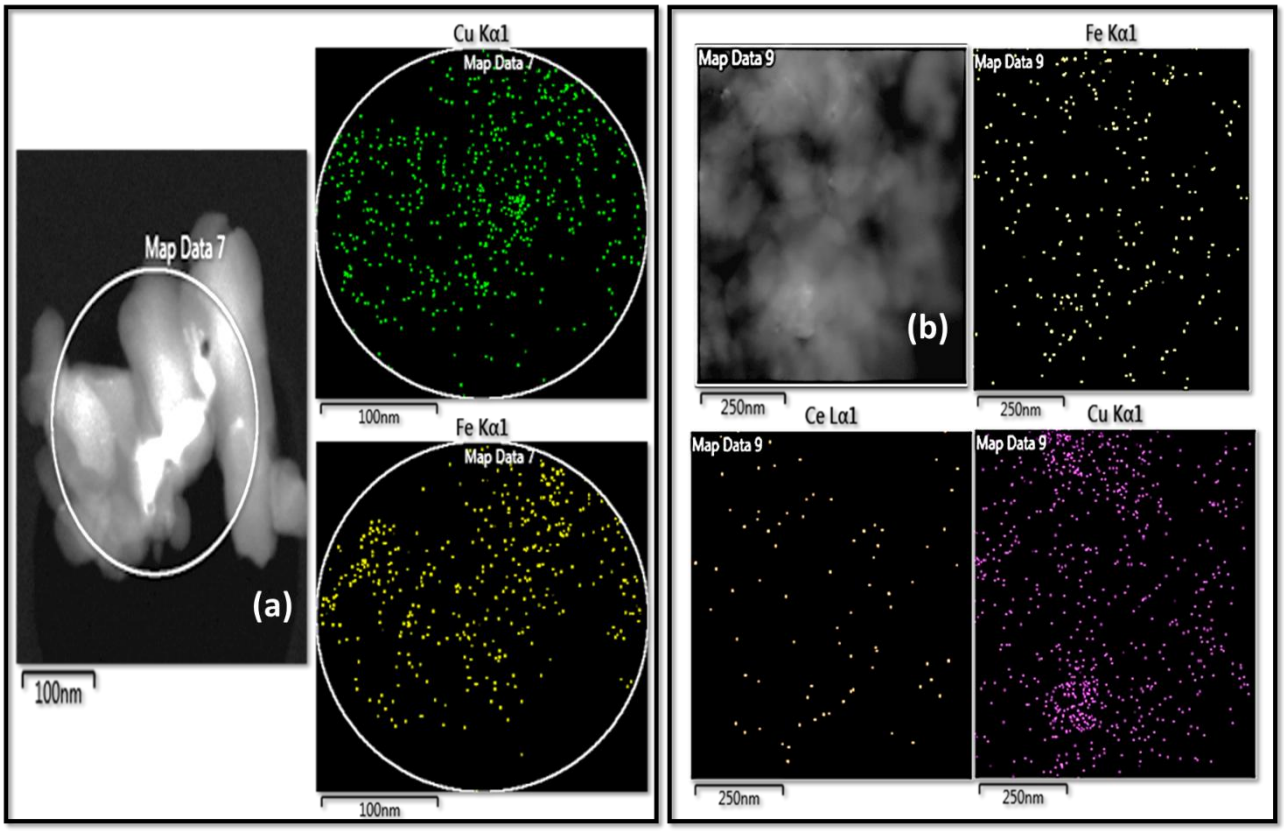

Fig. 7 EDX-STEM mapping images of (a) Fe-Cu-Z and (b) Ce-Fe-Cu-Z catalysts.

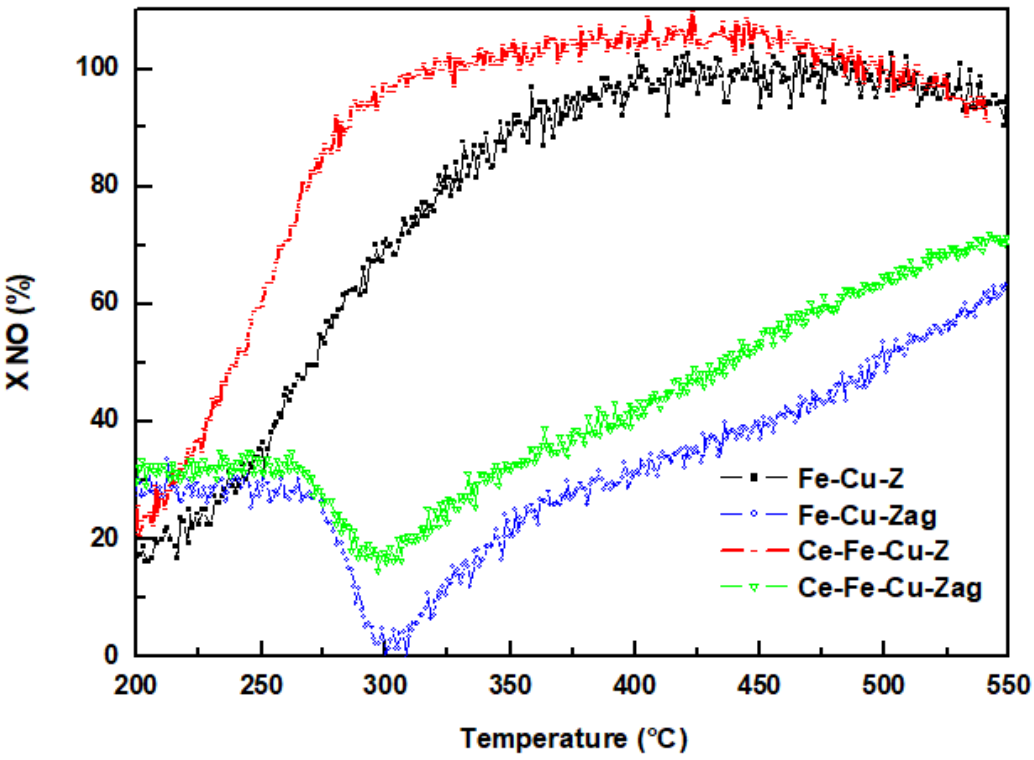

Fig. 8 NO conversion over fresh and aged catalysts.

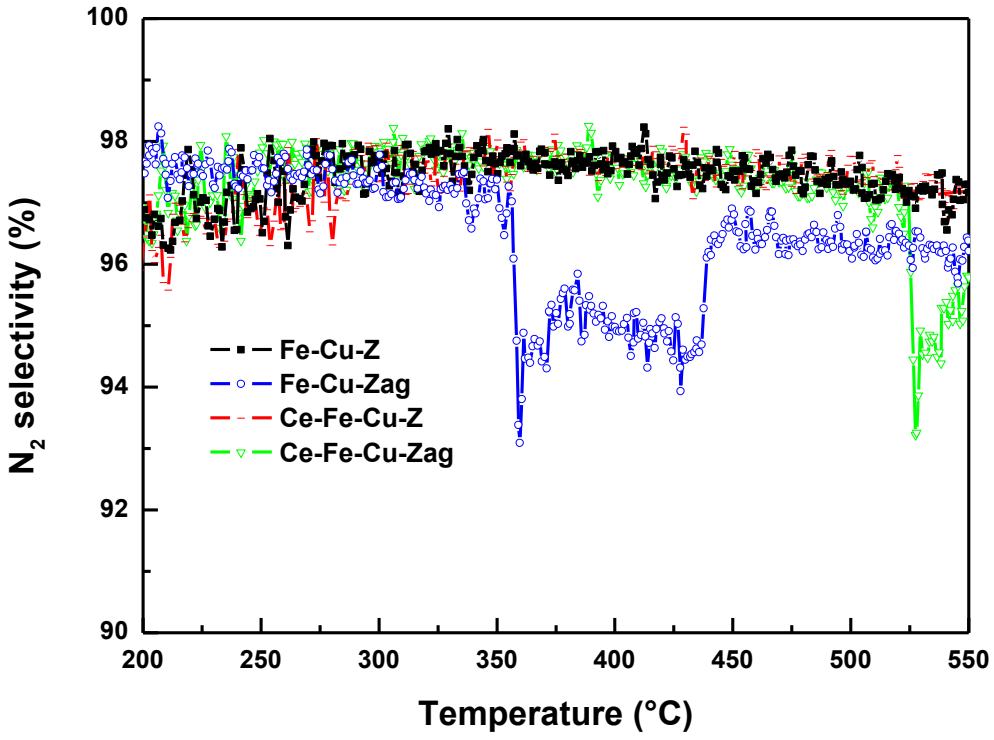

Fig. 9 N_2 selectivity over fresh and aged catalysts.

Table 1

ICP-AES chemical analysis results

Sample	Cu (wt.%)	Fe (wt.%)	Ce (wt.%)	Si/Al*	Cu/Al*	Fe/Al*	Ce/Al*
NH_4^+-ZSM-5	-	-	-	15	-	-	-
Fe-Cu-Z	1.40	1.82	-	13.23	0.23	0.33	-
Ce-Fe-Cu-Z	1.43	1.81	0.45	13.27	0.22	0.32	0.03

* Molar ratio

Table 2

N_2 physisorption at 77 K results.

Sample	S_{BET} [a] (m^2/g)	Pore volume (cm^3/g)	Micropore volume [b] (cm^3/g)
NH_4^+-ZSM-5	336	0.150	0.120
Fe-Cu-Z	327	0.130	0.110
Fe-Cu-Zag	291	0.092	0.046
Ce-Fe-Cu-Z	308	0.087	0.089
Ce-Fe-Cu-Zag	317	0.084	0.064

[a] calculated by BET method, [b] calculated by t-plot method

Table 3

EDX elemental analysis results

Sample	Spectrum	Element (wt.%)						
		O	Al	Si	Cl	Fe	Cu	Ce
Fe-Cu-Z	22	47,73	1,55	40,31	0,40	1,60	8,41	-
	25	54,85	0	26,32	0,33	18,50	0	-
	26	46,15	0	12,44	0,18	40,05	1,17	-
	27	51,87	1,95	33,41	1,18	10,61	0,98	-
	Map data 7	55,82	2,35	41,34	0	0,49	0	-
Ce-Fe-Cu-Z	29	58,27	0	37,61	1,26	2,55	0	0,3
	30	51,49	1,21	46,64	0,20	0,46	0	0
	38	48,51	2,33	40,62	1,97	0,23	6,34	0
	Map data 9	48,51	2,33	40,62	1,97	0,23	6,34	0